Arctic decadal variability from an idealized atmosphere-ice-ocean model:
2. Simulation of decadal oscillations

Dmitry Dukhovskoy,[1] Mark Johnson,[2] and Andrey Proshutinsky[3]

[1] A simple model of the Arctic Ocean and Greenland Sea, coupled to a thermodynamic sea ice model and an atmospheric model, has been used to study decadal variability of the Arctic ice-ocean-atmosphere climate system. The motivating hypothesis is that the behavior of the modeled and ultimately the real climate system is auto-oscillatory with a quasi-decadal periodicity. This system oscillates between two circulation regimes: the Anticyclonic Circulation Regime (ACCR) and the Cyclonic Circulation Regime (CCR). The regimes are controlled by the atmospheric heat flux from the Greenland Sea and the freshwater flux from the Arctic Ocean. A switch regulating the intensity of the fluxes between the Arctic Ocean and Greenland Sea that depends on the interbasin gradient of dynamic height is implemented as a delay mechanism in the model. This mechanism allows the model system to accumulate the "perturbation" over several years. After the perturbation has been released, the system returns to its initial state. Solutions obtained from numerical simulations with seasonally varying forcing, for scenarios with high and low interaction between the regions, reproduced the major anomalies in the ocean thermohaline structure, sea ice volume, and freshwater fluxes attributed to the ACCR and CCR.

1. Introduction
1.1. Motivation

[2] Analyses of Arctic sea ice, atmospheric, oceanic and hydrologic data indicate that the Northern polar region exhibits variability within a wide spectral range with seasonal, decadal, and interdecadal peaks [*Coachman and Aagaard*, 1988; *Mysak and Venegas*, 1998; *Deser et al.*, 2000; *Polyakov and Johnson*, 2000; *Rigor et al.*, 2000; *Venegas and Mysak*, 2000; *Proshutinsky et al.*, 2002]. There has always been motivation to find mechanisms that cause the observed changes in Arctic atmosphere-ice-ocean system [e.g., *Bradley and Miller*, 1972; *Budyko*, 1977; *van Loon and Rogers*, 1978; *Jones et al.*, 1986; *Mysak and Power*, 1992; *Wadhams*, 1994; *Dickson*, 1999; *Vinnikov et al.*, 1999; *Häkkinen and Geiger*, 2000]. In order to understand climate variability and its forcing, several indices have been introduced: the NAO index [*Walker*, 1924], the Arctic Ocean Oscillation (AOO) [*Proshutinsky and Johnson*, 1997], and the Arctic Oscillation (AO) index [*Thompson and Wallace*, 1998]. All indices reveal a quasi-decadal signal. The decadal positive and negative peaks in the NAO and AO time series, which are highly correlated, are manifested in changes of the Arctic atmosphere, sea ice and ocean [*Deser et al.*, 2000; *Dickson et al.*, 2000]. As an illustration, spectra of the AOO and AO indices are shown in Figure 1. The spectrum of the AOO has a significant peak at the 11.4 year period. The AO spectrum has two distinguishable peaks corresponding to periods of 2.7 and 10.8 years.

[3] The relationship between atmospheric, cryospheric, and oceanic variables and the AO, NAO, and AOO indices has been actively investigated [*Ambaum et al.*, 2001; *Rigor et al.*, 2002; *Hurrell et al.*, 2003; *Häkkinen and Proshutinsky*, 2004], motivated by the goal of deriving a "universal index" describing the behavior of the Arctic climate system. Whether such an index exists is an open question because systems change with time. Nevertheless, climate indices are often useful for identifying regimes of variability and mechanisms of climate change. Figure 2 illustrates one attempt to describe decadal variability of the Arctic climate system in terms of the AOO index. The figure shows a typical distribution of sea level atmospheric pressure and surface circulation for anticyclonic and cyclonic circulation regimes. There are two circulation cells during the ACCR: anticyclonic in the Arctic Basin and cyclonic in the Greenland-Iceland-Norwegian Sea (GIN Sea). During the ACCR, interaction (atmospheric and oceanic fluxes) between these

[1]Center for Ocean-Atmospheric Prediction Studies, Florida State University, Tallahassee, Florida, USA.
[2]Institute of Marine Science, University of Alaska Fairbanks, Fairbanks, Alaska, USA.
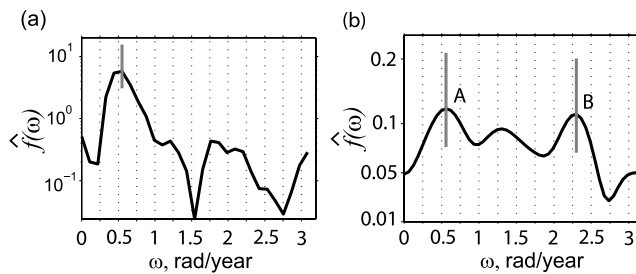[3]Physical Oceanography Department, Woods Hole Oceanographic Institution, Woods Hole, Massachusetts, USA.

Figure 1. Spectra of the AO (Figure 1a) and AOO (Figure 1b). The ordinate is the spectra estimate (logarithmic scale). The abscissa is frequency (rad·yr^{-1}). Time series of the AO and AOO are shown in Figure 2 (bottom panel). (a) The spectrum is calculated from the time series of detrended annual AOO index from 1946–2002 using the Tukey window with band width 0.279 rad·yr^{-1}. The vertical bar denotes 95% confidence interval of the peak with corresponding frequency $\omega = 0.551$ rad·yr^{-1} (11.4 years). (b) The spectrum is calculated from the time series of detrended annual AO index from 1900–2000 using the Tukey window with band width 0.419 rad·yr^{-1}. Vertical bars denote 95% confidence intervals of the two peaks A and B with corresponding frequencies $\omega = 0.582$ rad·yr^{-1} (10.8 years), and 2.3 rad·yr^{-1} (2.7 years). Monthly AO was acquired from the website of the Department of Atmospheric Science, Colorado State University: http://www.atmos.colostate.edu/ao/Data/ao_index.html.

regions is reduced. In contrast, during the CCR there is a single cyclonic circulation cell within the two basins and water exchange between them is intensified. The bottom figure shows time series of the AOO and the AO. Before 1978 the time series do not correlate, but after 1978 the indices are negatively correlated with the AOO anticyclonic and cyclonic regimes corresponding to the low and high indices of the AO, respectively.

[4] The reason for the abrupt switch in the AOO/AO relation is unclear. One idea relates to the lack of observational data over the Arctic prior to 1978 when the International Arctic Buoy Program began providing sea surface atmospheric pressure data for the central Arctic. Another explanation is that the AOO is a local index reflecting changes in the Arctic and sub-arctic only, while the NAO/AO indices are hemispheric in extent. In any case, when the Atlantic influence strengthens over the Arctic, the AOO correlates well with the NAO/AO. When this influence fades, the Arctic region is localized and the AOO has little relation to the NAO/AO indices. In the working hypothesis outlined below, the AOO is thought to reflect interactions inside the closed Arctic – GIN Sea climate system.

[5] Recently several conceptual models of Arctic climate variability have been introduced [*Ikeda*, 1990; *Mysak and Power*, 1992; *Mysak and Venegas*, 1998; *Ikeda et al.*, 2001; *Goosse et al.*, 2002; *Proshutinsky et al.*, 2002]. In these hypotheses, atmosphere-ocean interaction plays a crucial role in climate variability. In the above publications, one factor regulating climate change processes is the freshwater (ice and liquid water) flux from the Arctic Ocean to the North Atlantic, and the second factor is the atmospheric heat flux from the North Atlantic to the Arctic. Compelling

manifestations of this link between the Arctic and North Atlantic are (1) salinity anomalies that most probably originated in the Arctic [*Aagaard and Carmack*, 1989; *Häkkinen*, 1993] and traveled the subpolar gyre in the 1970s, 1980s, and 1990s [*Dickson et al.*, 1988; *Belkin et al.*, 1998]; (2) atmospheric warming and cooling events in the Arctic SAT that are related to the cyclone activity in the central and eastern Arctic [*Serreze et al.*, 1997; *Rigor et al.*, 2000] and coupled to the Arctic's atmospheric circulation [*Thompson and Wallace*, 1998].

1.2. Background

[6] The purpose of this study is to explore *Proshutinsky et al.*'s [2002] mechanism of Arctic climate variability characterized by the transition of the ACCR/CCR with a period of $10-15$ years. The studied climate system is viewed as a closed system following the idea mentioned above that the AOO index describes variability only within the Arctic basin and the GIN Sea. We focus on the description of possible auto-oscillations within an artificially closed Arctic Ocean – GIN Sea system.

[7] This study is based on the following working hypothesis summarized from *Proshutinsky and Johnson* [1997], *Proshutinsky et al.* [2002], and *Dukhovskoy et al.* [2004]. During the ACCR the Arctic Ocean-GIN Sea climate system is characterized by weak between-basin interaction: heat flux to the Arctic Ocean and freshwater flux to the GIN Sea are relatively low. Low heat flux to the Arctic leads to a colder Arctic atmosphere and a stronger anticyclone. This strengthens the wind-driven circulation of the Beaufort Gyre, increasing convergence of surface water and ice so that fresh water is retained in the gyre and potential energy builds. For this case, the upper Arctic Ocean is fresher and the atmosphere is colder than average. With weak interaction, freshwater outflow to the GIN Sea, via the East Greenland Current (EGC), is less than average. The reduction of fresh, buoyant surface water decreases water column stability and favors convection in the central Greenland Sea in winter. Strong convection and intense surface heat flux to the winter atmosphere cause positive SAT anomalies in the atmosphere above the GIN Sea and intensification of cyclonic vorticity [*Häkkinen*, 1995; *Mysak and Venegas*, 1998]. Thus, during the weak interaction state, the Arctic becomes colder and fresher, and the GIN Sea becomes warmer and more saline than average. This leads to growth of SAT and dynamic height gradients between these regions. Strong gradients ultimately promote interaction such that intense heat flux to the Arctic from the GIN Sea warms the atmosphere and weakens the Arctic anticyclone [*Serreze et al.*, 1997] resulting in the shift to the CCR.

[8] The CCR is characterized by strong interaction (intense freshwater and heat fluxes) between the basins. Anticyclonic circulation in the Beaufort Gyre weakens, and fresh water is released to the GIN Sea. The upper layer of the central Greenland Sea becomes fresher, increasing vertical stability and suppressing convection [*Aagaard and Carmack*, 1994]. Without entrained oceanic heat from below, the mixed layer in the central Greenland Sea easily reaches the freezing point in winter, enhancing ice formation [*Häkkinen*, 1995; *Pawlowicz*, 1995]. Both weak convection and ice cover reduce the heat flux to the winter atmosphere, which then cools, and cyclonic vorticity
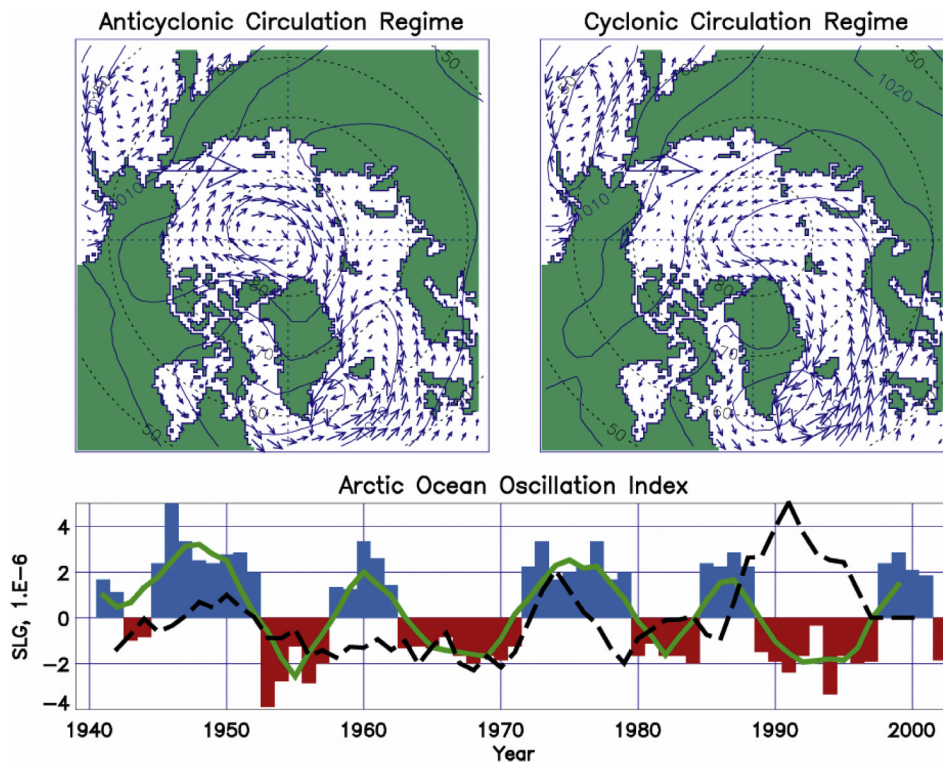
Figure 2. Arctic Ocean Oscillation (AOO) index from updated results of *Proshutinsky and Johnson* [1997]. The top left and right figures show typical distribution of sea level atmospheric pressure and surface circulation for anticyclonic and cyclonic circulation regimes, respectively. There are two circulation cells during the ACCR: anticyclonic in the Arctic Basin and cyclonic in the GIN Sea and the interaction between these regions is reduced. During the CCR, there is a single cyclonic circulation cell within these two basins and the water exchange among basins is intensified. The bottom figure shows time series of the AOO and AO. Blue and red bars show annual AOO with blue corresponding to the ACCR and red depicting the CCR years. The green solid line shows a 5-year running mean of the AOO. The black dashed line delineates a 5-year running mean winter AO from D. Thompson's web site (http://www.tao.atmos.washington.edu/ao). The AO and AOO negatively correlate during the last 20 years, but before 1978 their correlation is weakly positive.

decreases [*Mysak and Venegas*, 1998]. After several years of intense interaction, interbasin SAT and dynamic height gradients have eroded, and the interaction fades. The CCR transits to the ACCR and the system then rebuilds the gradients between regions. The proposed relationships between the Arctic and GIN Sea subsystems for low (ACCR) and high (CCR) interaction rates are summarized in Figure 3.

1.3. Dynamic Height Gradient

[9] The ACCR and CCR are characterized by increasing and decreasing dynamic height gradients between the Arctic Ocean (Beaufort Gyre) and the Greenland Sea. The *Environmental Working Group* (*EWG*) [1998] atlas provides annual fields of dynamic heights for the Arctic Basin. Although the EWG does not show dynamic heights for the most of the GIN Sea, the available fields suffice to analyze changes in dynamic height gradient which regulate fluxes via Fram Strait. Figure 4 shows EOF analysis of these dynamic heights. The first EOF mode describes 59% of the variability and oscillates with approximately a 10-year

period. The first EOF pattern shows that when the dynamic heights increase in the Nansen and Amundsen basins (warming or freshening) the dynamic heights decrease in the adjacent region (cooling or salinization) and vice versa. These results show that thermohaline structure of the upper Arctic Ocean has noticeable decadal variability [see also *Moon and Johnson*, 2005]. In this study, it is hypothesized that these decadal oscillations of the dynamic heights in the Arctic Ocean are related to the decadal cycle of the ACCR/CCR transitions. During the ACCR, dynamic height in the central Arctic increases and in the adjacent area decreases resulting in strong dynamic height gradients that force water away from the central Arctic Ocean. During the CCR, freshening and warming of the upper Arctic Ocean and release of fresh water from the central Arctic Ocean lead to leveling the dynamic heights over the basin and decreasing the dynamic height gradient.

1.4. Model Outline

[10] An idealized box-based model of the Arctic Ocean and GIN Sea has been developed, calibrated and validated.
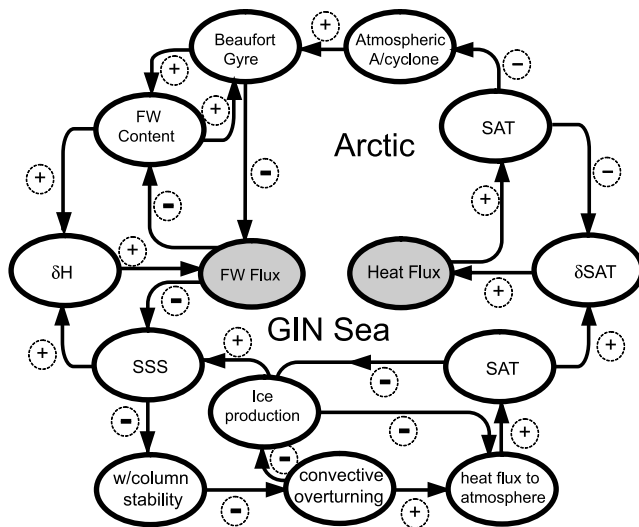
Figure 3. Interaction loop in the Arctic climate system. The upper and lower diagrams show Arctic and GIN atmosphere-ice-ocean systems, respectively. A plus sign denotes mechanisms with positive result between two cells (increase/decrease in one cell causes increase/decrease in second), a minus sign denotes mechanisms with negative results (increase/decrease in one cell causes decrease/ increase in second). Interaction between the two regions is performed through oceanic and atmospheric fluxes (grey cells). See text for details. Note that FW flux to the GIN Sea is controlled by two oppositely acting mechanisms: convergence of freshwater in the Beaufort Gyre during the ACCR makes less freshwater available for export to the GIN Sea, but on the other hand, FWC in the Arctic Ocean (mostly the Beaufort Gyre) increases, leading to a stronger gradient of dynamic height between the two basins which forces higher outflow to the GIN Sea. δH is the interbasin gradient of dynamic height. δSAT is the interbasin gradient of SAT.

A detailed description of the model and its validation are presented in part 1 of this paper [*Dukhovskoy et al.*, 2006], so only a brief description is provided here.

[11] The Arctic module includes an Arctic Ocean model coupled to a thermodynamic sea ice model, a sea-ice shelf model, and an atmospheric box model. The Arctic Ocean model is one-dimensional, three-layer and time-dependent. This is the Arctic Ocean model of *Björk* [1989] with modified entrainment velocity, shelf inflow/outflow and improved shelf – interior basin interaction. The three layers are: the mixed layer, halocline layer, and Atlantic layer. The model describes deepening and shallowing of the mixed layer, and temperature and salinity changes in the mixed layer and halocline. The characteristics of the Atlantic layer do not change. The atmospheric box model estimates SAT from the total energy balance, with interannual variability induced by varying heat flux, F_{adv}, from the Greenland Sea atmospheric box. F_{adv} is a function of the SAT gradient (δSAT) between the Arctic and the Greenland Sea modules. The Greenland Sea ocean model is one-dimensional and time dependent and is, in general, similar in structure to the Arctic Ocean model. The model layers follow *Swift* [1986]. The oceanic model is coupled to a thermodynamic sea ice model and an atmospheric model. The atmospheric model calculates SAT anomalies for the computed surface heat flux. The Greenland Sea module describes the seasonal and interannual variability of the heat content of the GIN Sea region by assuming it is related to the air-sea surface heat flux. The air-sea heat flux, in turn, is determined by the intensity of convection in the Greenland Gyre which is controlled by the amount of fresh water (FW) advected from the Arctic Ocean. As discussed above, the dynamic height gradient between the Arctic Ocean and the Greenland Sea characterizes and regulates the oceanic interaction, and the surface air temperature gradient between the two regions is responsible for interaction between the atmospheric boxes.
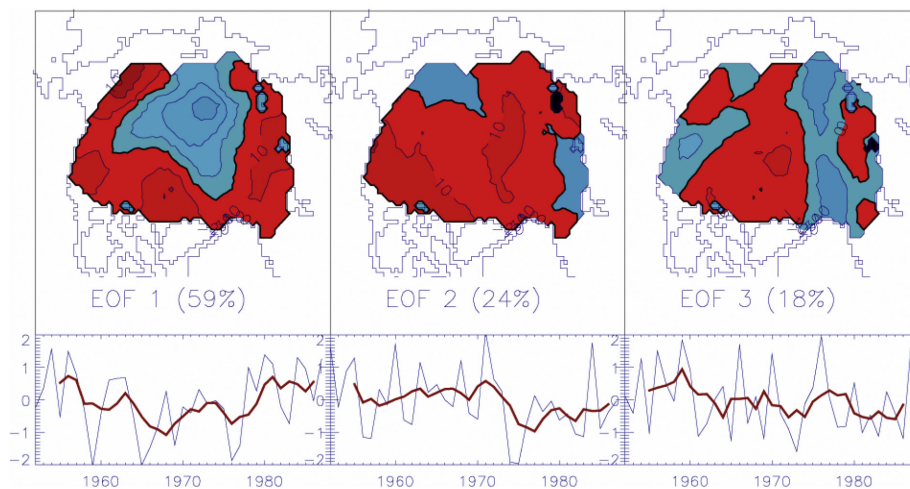

Figure 4. EOF analysis of the dynamic heights in the Arctic Ocean. In the EOF fields, blue regions indicate negative and red regions indicate positive anomalies. Time series of principle components of the EOFs are shown at the bottom (blue curves) with a 5-year running mean (red). The EOF-1 pattern shows that maximum variability occurs in the Nansen and Amundsen basins with a period of approximately 10 years.

Table 1. Annual and Decadal Variability of Forcing Parameters

Parameters	Seasonality	ACCR/CCR Forcing
Arctic domain		
Solar radiation	Yes	No
Relative humidity	Yes	No
Ice/snow albedo	Yes	No
Wind	Yes	Yes
Cloudiness	Yes	Yes
Bering Strait inflow	Yes	No
Shelf-interior Arctic Ocean water exchange, Q_{mao}, Sv	No	No
Outflow from the Arctic Ocean to the Greenland Sea model, $Q^*_{g\_atl}$	Simulated	Yes
Ice volume flux from the Arctic Ocean, V_{flx}, Sv	Yes	Yes
Coefficient of heat advection, χ, W·m^{-2}·$^\circ$K^{-1}	No	Yes
Proportionality coefficient that parameterizes dissipation of forced convection in the entrainment formula (equation (6), part 1), m_0	No	No
Proportionality coefficient that parameterizes dissipation of free convection in the entrainment formula (equation (6), part 1), κ	No	No
Shelf domain		
Solar radiation	Yes	No
Relative humidity	Yes	No
Ice/snow albedo	Yes	No
Wind	Yes	Yes
River runoff	Yes	No
Cloudiness	Yes	Yes
Net precipitation	Yes	No
Greenland Sea domain		
Solar radiation	Yes	No
Relative humidity	Yes	No
Ice/snow/sea albedo	Yes	No
Wind	Yes	Yes
Proportionality coefficient that parameterizes dissipation of forced convection in the entrainment formula (equation (6), part 1), m_0	No	No
Proportionality coefficient that parameterizes dissipation of free convection in the entrainment formula (equation (6), part 1), κ	No	No
Polar water flux, Q_{PW}	Yes	Yes
Polar water temperature, T_{PW}	Simulated	Simulated
Polar water salinity, S_{PW}	Simulated	Simulated
Atlantic water inflow, Q_{Atl}	Yes	No
Atlantic water temperature, T_{Atl}	Yes	No
Atlantic water salinity, S_{Atl}	No	No
Ice volume flux, $Q_{mlt\ GS}$	Yes	Yes

[12] The described model is a lucid application of the real Arctic climate system. Although using an idealized model requires simplifying a complex problem, a simple model has several advantages. One can easily track the propagation of perturbation signals within the system, analyze simulated behavior to test the hypothesis, and detect flaws in the proposed mechanism. Also it is noteworthy that the reliability of complex models is imperfect. The ability of Arctic Ocean models to simulate variability on seasonal and interannual time scales is still unclear, as many models contradict each other when simulating the vertical structure in the Beaufort Gyre, the circulation of Atlantic water in the Arctic Basin, and the salinity and freshwater content (FWC) of the Arctic Ocean [*Proshutinsky et al.*, 2001, 2005; *Steele et al.*, 2001].

2. Model Forcing, Initialization, and Spin-Up

[13] *Proshutinsky et al.* [1999] and *Polyakov et al.* [1999] have shown that the annual variability of the Arctic climate is characterized by a large seasonal cycle against a background of climatically significant decadal and interannual variability. In order to reproduce decadal variability correctly, we have parameterized the major forces where possible

in accordance with the two different climate regimes. Model forcing is specified via solar radiation, wind stress, river runoff, Atlantic and Bering Strait inflows, cloudiness, air humidity, and ice/snow albedo. External and internal parameters regulating the forcing and interaction rates are summarized in Table 1. Characteristics of forcing variables and their parameterization for decadal variability are described in this section.

2.1. External Forcing
2.1.1. Wind
[14] In general, wind speed in the Arctic is higher during the CCR [*Polyakov et al.*, 1999; *Rigor et al.*, 2002] and the maximum difference between the ACCR and CCR wind speed is observed in the central Arctic and in the Greenland Sea regions [*Polyakov et al.*, 1999]. We used the NCEP Reanalysis monthly surface wind speed for the central Arctic and the Greenland Sea from the National Oceanic and Atmospheric Administration (NOAA) – Cooperative Institute for Research in Environmental Sciences (CIRES) Climate Diagnostic Center (CDC) (http://www.cdc.noaa.gov) to estimate the long-term monthly mean wind speed and its variance. Following *Polyakov et al.* [1999] (see their Figure 4), during the CCR the annual wind speed in the
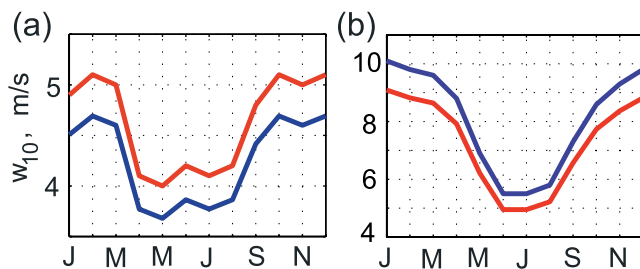
Figure 5. Monthly wind speed for the ACCR (blue) and CCR (red) used in the model experiment for Arctic module (a) and Greenland Sea module (b). The abscissa is months.

Greenland Sea is ∼0.9 of that during the ACCR, and the ACCR wind in the central Arctic is ∼0.9 of the CCR wind. In this model experiment, monthly wind speeds are set to be one standard deviation above the corresponding long-term monthly mean for high wind and one standard deviation below the mean for low wind. Idealized wind speeds used in our simulations for different regimes are shown in Figure 5.

2.1.2. Cloudiness

[15] Cloudiness influences the heat balance in the Arctic [*Beesley and Moritz*, 1999]. Based on observed 3-hour cloud observations and surface air temperatures measured on the Russian ice drifting station NP-4, *Makshtas et al.* [1999] established a strong positive cross-correlation between the surface air temperature and cloudiness. Thus, in warm years the frequency of overcast skies increases. During cold years, the number of days with clear skies increases. Similarly, *Polyakov et al.* [1999] argued that during the CCR (positive SAT anomalies) the Arctic sky, in general, had more clouds. *Beesley* [2001] reported a correlation between surface air temperature cold anomalies and the low-cloud fraction, although the mechanism behind this relationship was unclear. In this experiment, we assume that cloudiness changes slightly under the two different climate regimes. Based on monthly mean values of cloudiness in the Arctic from *Lindsay* [1998] and *Gorshkov* [1980] and assuming that there is slightly lower cloudiness during the ACCR [*Polyakov et al.*, 1999], the Arctic cloudiness parameterization presented in Figure 6 was applied to force the Arctic Ocean model. Unfortunately, the available data sets of cloudiness for high latitudes are too uncertain and scattered to obtain reliable estimates for the average cloud cover in the Arctic for different regimes.

[16] No evidence for a relationship between the AOO or the NAO/AO and cloudiness in the GIN Sea region has been found in the scientific literature. Thus, in the simulation, cloudiness in the Greenland Sea has only seasonal but no interannual variability.

2.2. Internal Parameters

[17] A set of internal model parameters regulates the system behavior (mainly the rates of heat and freshwater exchange among different model domains) depending on the circulation regime. The characteristics of these parameters are described below.

2.2.1. Heat Flux to the Arctic

[18] The heat flux to the Arctic (F_{adv}) depends on the SAT difference between the Arctic and Greenland Sea modules and on the coefficient of heat advection, χ (equation (25),

part 1). Based on sensitivity experiments, this coefficient is set to $\chi = 1.5$ W·m^{-2}·°K^{-1} during the ACCR and $\chi = 2.4$ W·m^{-2}·°K^{-1} during the CCR. As explained in *Marotzke and Stone* [1995], the coefficient parameterizes the intensity of meridional sensible heat transport to high latitudes by transient eddies. There is evidence in the literature that warming and decrease in the mean sea level pressure (SLP) in the Arctic is attributed to the intensification of cyclone penetration into the Arctic [*Maslanik et al.*, 1996; *Serreze et al.*, 1997]. There is a link between cyclone activity and the NAO [*Rogers*, 1997; *Serreze et al.*, 1997] that is consistent with our hypothesis that during the cyclonic regime in the Arctic the meridional heat advection to this region from the GIN Sea is higher. The full relationship among cyclone activity in the Arctic Ocean – GIN Sea region, SLP, and the NAO/AO is still under discussion [see *Dickson et al.*, 2000].

2.2.2. Water Flux From the Arctic Basin to the GIN Sea

[19] The water outflow from the Arctic module to the GIN Sea module (Q_{g_atl}) is assumed to occur as a geostrophically balanced current [*Björk*, 1989]. An estimate of the outflow at each level in a geostrophic outlet is obtained by integrating the thermal wind equation across the flow (see part 1 for details). In other words, the thermohaline structure of the upper ocean across the geostrophical outlet (Fram Strait) determines the vertical structure of the flow. This approach addresses the flow driven by the density gradients but it does not take into account local winds, probably the most important feature of water and ice exchange between the two basins [*Vinje and Finnekasa*, 1986; *Häkkinen*, 1993; *Kwok and Rothrock*, 1999]. The effects of local winds are reflected in the different outflow rates of the Arctic Ocean water to the Greenland Sea under the different circulation regimes [*Proshutinsky and Johnson*, 1997; *Proshutinsky et al.*, 1999, 2002]. The model study of *Polyakov et al.* [1999] indicates a twofold increase of the Arctic Ocean water export to the Greenland Sea in the upper 200 m during the CCR compared to the ACCR. In order to take the effects of local winds into account in our model, the ocean model calculated outflow from the Arctic Ocean (Q_{g_atl}) is relaxed to higher and lower outflow rates during different climate regimes:

$$Q_{g\_atl}^* = \begin{cases} 0.7 \cdot Q_{g\_atl}, & ACCR \\ 1.5 \cdot Q_{g\_atl}, & CCR \end{cases}, \qquad (1)$$
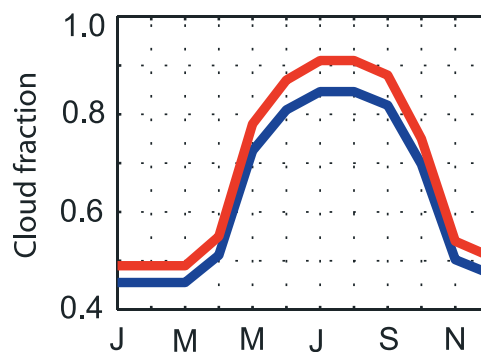

Figure 6. Cloudiness in the Arctic module for the ACCR (blue) and CCR (red). The abscissa is months.
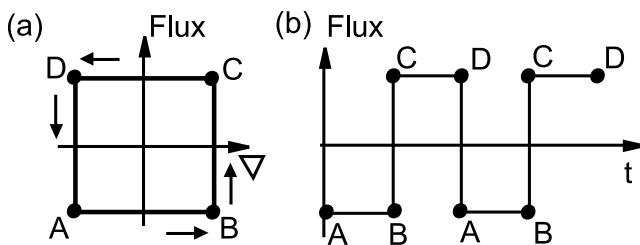
Figure 7. Step function parameterizing high and low fluxes between the Arctic and GIN Sea in the model climate system. (a) Fluxes are kept low (A-B) during the weak interaction state until the gradients (∇) reach the upper threshold (point B). Fluxes are set high while the gradients decrease (C-D). When the gradients are at the lower threshold value (point D) the fluxes are set low. (b) Time series of the step function with flux on the ordinate.

When the regime shifts, the outflow Q_{g_atl} is relaxed to $Q^*_{g\_atl}$ with a time scale of 3 years. The time scale is roughly estimated from the average time required for a water parcel to travel from the Beaufort Gyre to the Greenland Sea (~2900 km) with an average speed of 0.03 m·s^{-1}. The amount of freshwater inflowing into the Greenland Sea domain is determined by the polar water volume flux (Q_{PW}). As explained in part 1, Q_{PW} is the fraction of the Arctic Ocean outflow $Q^*_{g\_atl}$ integrated from the surface to 150 m depth. Hence, Q_{PW} has both seasonal and interannual variability (Table 1).

2.2.3. Ice Volume Flux to the Greenland Sea

[20] Ice from the EGC and Jan Mayen Current is advected into the central Greenland Sea [*Swift*, 1986; *Aagaard and Carmack*, 1989; *Vinje et al.*, 2002] but the rate of supply is uncertain. *Swift* [1986], having analyzed tritium data from the Greenland and Iceland Seas, argued that even if ice from the EGC or Jan Mayen Current is incorporated into the Greenland Gyre, the supply rate must be low. Summer is the most favorable season for ice advection into the central Greenland Sea when the cyclonic vortex is weak and the ice is highly mobile. In the cold season, intensified cyclones force surface water and ice from the central Greenland Sea. The necessity of including the ice volume flux (Q_{mlt_GS}) in the model was partly dictated by a surplus of energy indicated by slightly warmer than climatology summer sea surface temperatures in the Greenland Sea model. Q_{mlt_GS} is estimated as a small fraction (5%) of the ice volume flux through Fram Strait. The fraction of ice advected into the central Greenland Sea is speculative and mostly based on *Aagaard and Carmack* [1989], who estimated that about 3% of the annual freshwater load entering through Fram Strait penetrates into the central Greenland Sea. The estimated ice volume flux through Fram Strait ranges from 0.06 to 0.16 Sv [*Kwok and Rothrock*, 1999] depending on value of the NAO index: a high flux during a positive index and a low flux during a negative NAO index (see also *Hilmer and Jung* [2000] for more discussion on the relation between the NAO and ice export). Based on the working hypothesis, lower ice advection to the Greenland Sea is attributed to the

ACCR and higher ice advection is attributed to the CCR:

$$
Q_{mlt\_GS} = \begin{cases} 0.05 \cdot V_{flx} \cdot \sin\left[\dfrac{\pi(d_j - 145)}{108}\right], & if \quad 145 \leq d_j \leq 253, \\ 0, & otherwise, \end{cases} \quad (2)
$$

where V_{flx} is ice volume flux (0.16 Sv for CCR and 0.06 Sv for the ACCR) and d_j is a day of year.

2.3. Parameterization of Regime Shifts and Model Spin-Up

[21] In order to generate self-sustained oscillations, a system should perform a delayed response to the changes caused by positive/negative feedback processes (see study on delayed oscillator in *Suarez and Schopf* [1988]). Our preliminary model experiments (results are not presented here) revealed that if the interaction (FW and atmospheric heat fluxes) is set proportional to the gradients without delay, no oscillations arise: the system rapidly achieves the steady state. For the model to oscillate, we specify that after the interbasin oceanic dynamic height gradient (δH) reaches some high critical value (δH_{max}), the interaction increases, gradients begin to weaken, and interaction continues until a minimum critical value (δH_{min}) is reached. So, the system oscillates between the two states: strong interaction during the CCR and weak interaction during the ACCR. Such behavior has been parameterized by a step function (Figure 7).

[22] When δH reaches δH_{min} the regime alters to anticyclonic (ACCR) and ACCR forcing values are set to characterize a cold Arctic climate state. The model is run with ACCR forcing until δH reaches δH_{max}. Then the parameters are changed to those characterizing a warm climate state in the Arctic (CCR forcing). The minimum and maximum threshold values (dashed lines in Figure 8a) have been determined from 20-year sensitivity runs with high and low FW and heat fluxes (weak and strong interaction) between the Arctic and Greenland Sea modules.

[23] The model is run for 110 years with the first 10 years of spin-up. After the 10-year spin-up, δH controls regime shift as described above.

3. Results: Decadal Variability in the Atmosphere, Ice, and Ocean Components

3.1. Dynamic Height and SAT Gradients

[24] The simulated Arctic Ocean – Greenland Sea climate system reproduces the hypothesized auto-oscillatory behavior. Figure 8 shows time series of the annual interbasin gradients of the dynamic height and SAT. In the simulation, the regimes shift with a period ranging from 10 to 15 years. The annual mean dynamic height gradient (δH) oscillates and slightly overshoots the upper and lower limits δH_{max} and δH_{min} (dashed lines). The system reveals some internal variability: during one cycle (e.g., year 29) δH starts increasing as soon as it has reached δH_{min}. During another cycle (e.g., year 89), δH keeps decreasing one more year after the regime has shifted. This is because any
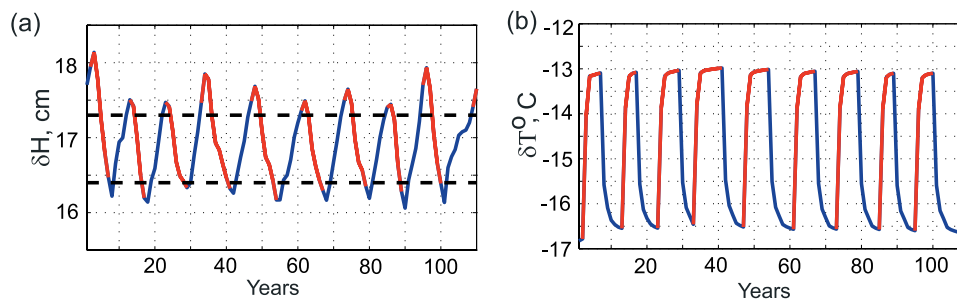
Figure 8. Time series of the ACCR/CCR. Different regimes are highlighted with red (CCR) and blue (ACCR). (a) Annual mean dynamic height gradient between the Arctic Ocean and the Greenland Sea. The black dashed lines are minimum and maximum δH. (b) Annual mean SAT gradient. The model reproduces auto-oscillatory behavior of the climate system with a period 10–15 years.

changes in the halocline density affect the dynamic height gradient and the halocline adjusts slowly to rapidly changing forcing parameters (heat advection, SAT, shelf inflow). Having a different response frequency than the forcing parameters, the halocline causes low-frequency variations in the system.

3.2. SAT and Surface Heat Flux

[25] Selected output from the atmospheric model is presented in Figure 9. The simulated SAT in the Greenland Sea (Figure 9a) lies within the 98% confidence interval of the means estimated from NOAA – CIRES CDC NCEP reanalysis SAT for the period 1948–2001 (http://www.cdc.noaa.gov). The Greenland Sea modeled SAT shows warmer winter and earlier spring during the modeled ACCR compared to the CCR. This is due to the different surface heat fluxes (F_{tot}) during the ACCR and CCR (Figure 9c). The significant reduction of the heat flux from late December through mid-April stems from the presence of the ice cover in the Greenland Sea during the CCR. Lower heat flux to the atmosphere causes negative SAT anomalies in the model (equation (36), part 1). During the ACCR, the situation is opposite – rapid deepening of the mixed layer entrains heat from below and releases it to the atmosphere resulting in a larger winter surface heat flux (Figure 9c). Large F_{tot} induces winter SAT warming in the Greenland Sea (Figure 9a).

[26] The differences between the simulated ACCR and CCR SATs are larger in the Arctic than in the Greenland Sea (Figure 9b). Simulated spring SAT (April) in the Arctic has a negative bias compared to the NCEP reanalysis SAT. Computed May SAT during the ACCR are outside the 98% confidence interval. In the Arctic, due to colder SAT during the ACCR, there are slightly higher fluxes to the atmosphere in winter and lower fluxes to the ocean in summer, compared to the CCR (Figure 9d).

3.3. Ice and Ocean Characteristics of the Arctic Ocean and Shelf

3.3.1. Arctic Ocean

[27] The results from the Arctic Ocean model are presented in Figures 10 and 11. The time series of the annual mean mixed layer depth (h_{ml}) (Figure 10a) shows shallowing of the mixed layer during the CCR and deepening during the ACCR. Such behavior comes from the lower entrainment velocities (w_e) during the CCR and higher w_e

during the ACCR (Figure 10c). The entrainment, in turn, depends (equation (6), part 1) on the reduced gravity (g') which is a function of the mixed layer salinity (S_{ml}) (Figure 10b) and buoyancy flux which is lower during the warm, cyclonic regime (not shown). During the ACCR, S_{ml} increases and the upper water column stability weakens, promoting a higher entrainment rate. The opposite sequence of events occurs during the CCR.
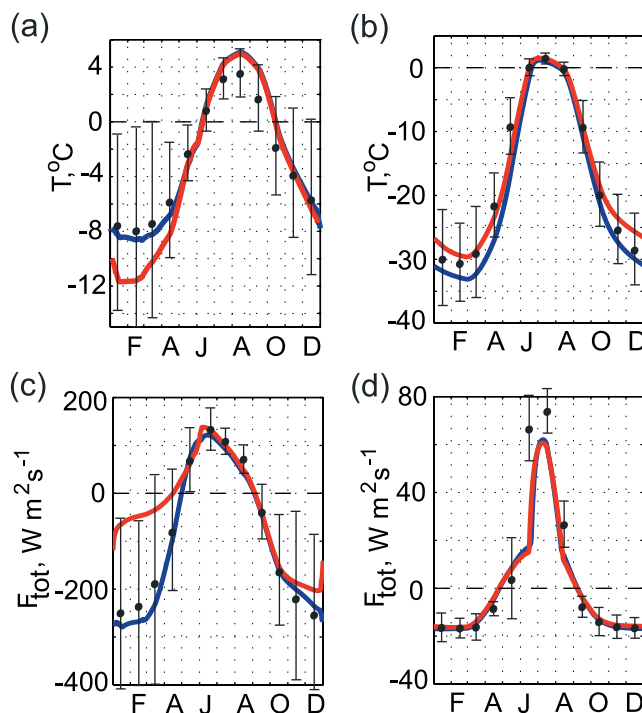

Figure 9. Time series of simulated daily SAT in the Greenland Sea (a) and the Arctic Ocean (b) averaged over the last years of forcing for the ACCR (blue lines) and CCR (red lines). The black dots on the vertical bars denote monthly mean values and their 98% confidence intervals, respectively. The estimates of the monthly means and their STD are obtained from NOAA-CIRES CDC data over the period 1948–2001. The abscissa is time, in months. (c) Same as Figure 9a, but for the Greenland Sea surface heat flux. (d) Same as Figure 9b, but for the Arctic Ocean surface heat flux.
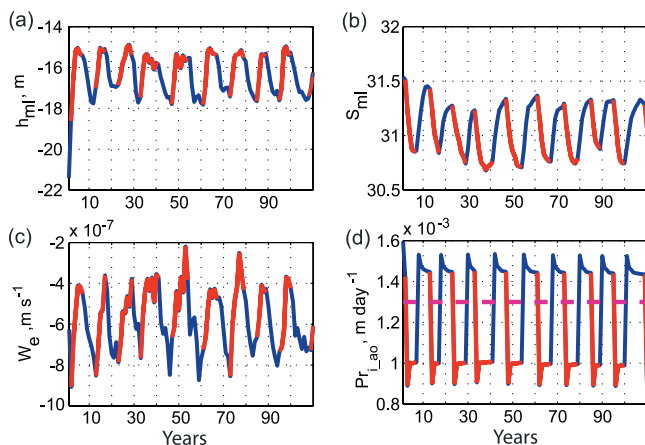
Figure 10. Time series of annual diagnostics from the Arctic Ocean model. Blue segments denote the period of ACCR forcing, red segments – CCR forcing. The abscissa is time, in years of integration. (a) Mixed layer depth. (b) Mixed layer salinity. (c) Entrainment velocity. (d) Ice production. Magenta dashed line shows annual ice production estimated by *Hibler* [1979].

[28] The model shows decadal variability of mixed layer salinity (S_{ml}) (Figure 10b). S_{ml} is rising during the ACCR and declining during the CCR. This is explained in part by the higher ice production (Pr_{i_ao}), (Figure 10d) which is from the lower SAT for the anticyclonic years (Figure 9b). Variation of the interannual ice thickness simulated in the model varies from 2.18 to 2.38 m or about 9% which is in agreement with *Thomas et al.* [1996]. Also shown (dashed line in Figure 10d) is the annual mean ice production obtained from *Hibler* [1979]. During the ACCR the model simulates higher ice production than Hibler's estimate and lower production during the CCR. This is quite reasonable because Hibler's result reflects the mean climate and mean ice production rates.

[29] In the model, outflow from the Arctic Ocean mixed layer varies from 1.2×10^5 m^3·sec^{-1} at the end of the anticyclonic regime to 2.8×10^5 m^3·sec^{-1} at the end of the cyclonic regime. Using salinity of the Atlantic layer (S_{atl} = 34.8) as a reference salinity and taking the average salinity of the mixed layer at the end of the ACCR to be 31.31 and at the end of the CCR to be 30.78, the amount of liquid fresh water exported from the Arctic Ocean mixed layer is 0.12×10^5 m^3·sec^{-1} at the end of the ACCR and 0.32×10^5 m^3·sec^{-1} at the end of the CCR. The higher freshwater flux from the mixed layer at the end of the CCR stems from higher outflow and its lower salinity.

[30] Model results show that water temperature and salinity (T/S) characteristics of the Arctic Ocean and Greenland Sea undergo significant changes under different climate regimes. Calculated characteristics (temperature, salinity, and σ-density) of the vertical structure of the upper 100 m for the Arctic Ocean are presented in Figure 11. Seasonal changes in the simulated Arctic Ocean take place in the upper 30–35 m. Interannual variability spreads deeper to approximately 150 m with amplitude fading with depth. As discussed earlier, the mixed layer is fresher (see also Figure 10b) and the halocline is barely more saline

during the CCR. However, the temperature difference is more obvious between the ACCR and CCR. Furthermore, the Arctic Ocean halocline is colder during the ACCR, a fingerprint of the shelf outflow. During the ACCR ice production on the shelf is higher and the shelf contributes more cold water (at the freezing point) to the halocline. From the model formulation (part 1, section 2.2), the shelf water is isopycnally mixed with the halocline water. Under these circumstances, the shelf inflow to the halocline does not change the density. At a given depth (density), halocline water is warmer and saltier than the shelf water of the same density. Nevertheless, the salinity difference is not significant, but temperature differs significantly. During the ACCR the shelf pumps cold (and less saline for given density) water into the halocline.

[31] The FWC in the simulated mixed layer and upper halocline undergoes interesting changes during the ACCR and CCR. Although the simulated mixed layer is fresher during the CCR winter (solid red profile in Figure 11a) than during the ACCR (solid blue profile), the layer is thicker during the ACCR winter. This leads to higher FWC in the mixed layer at the end of ACCR winter (14,724 km^3 of fresh water) compared to the CCR (12,147 km^3 of fresh water). In summer, when the mixed layer thickness is of the same magnitude during both regimes (∼12 m), the FWC during the CCR is higher (10,096 km^3 of fresh water) compared to the ACCR (9,044 km^3 of fresh water). Significant fresh water is stored in the seasonal halocline (approximately 16,196 km^3 and 18,650 km^3 at the end of ACCR and CCR summers, respectively). The annual mean FWC in the mixed layer is increasing during the ACCR and, by the end of the regime, it reaches 10,828 m^3 of liquid fresh water. During the CCR, the annual FWC is decreasing towards 10,700 m^3 by the end of the CCR.

[32] The FWC of the modeled halocline (below the seasonal halocline) does not reveal seasonality. Although ACCR salinity in the halocline is only slightly lower than that during the CCR, the difference in the FWC of the
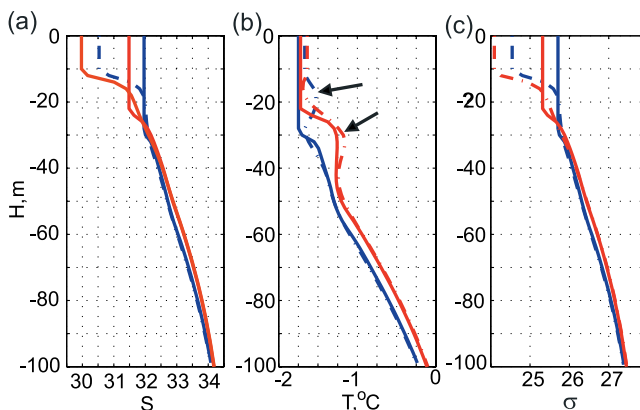

Figure 11. Vertical structure of the upper layer of the simulated Arctic Ocean under different regimes. Blue curves correspond to ACCR forcing, red lines to CCR. Solid lines are April profiles, dashed-dotted lines are September profiles. The ordinate is depth. (a) Salinity. (b) Temperature. Arrows indicate "bulges" due to Bering water inflow. (c) σ-density.

Table 2. Freshwater Storage (km^3) in the Simulated Arctic Ocean During Different Regimes

	ACCR		CCR	
Layer	Summer	Winter	Summer	Winter
Mixed layer	9,044	14,724	10,096	12,147
Seasonal halocline	16,196	-	18,650	-
Base of the winter mixed layer to 100 m	22,086	22,086	20,771	20,771
100 m − 200 m	7,011	7,011	7,011	7,011
In all	54,337	43,821	56,528	39,929

halocline is more noticeable. In the depth interval from the base of the seasonal halocline (30 m for the ACCR and 21 for the CCR) to 100 m (below 100m the difference between salinity profiles for different regimes is indistinguishable) the FWC is 22,086 km^3 and 20,771 km^3 during the ACCR and CCR, respectively. The halocline below 100 m contributes an additional 7,011 km^3 of fresh water. In all, from the model diagnostics, the upper 200 m of the Arctic Ocean contains more fresh water during CCR summer due to higher melt rates. The FWC in the upper 200 m is 54,337 km^3 and 56,528 km^3 of liquid fresh water during the ACCR and CCR summers, respectively (Table 2). These values are close to *Aagaard and Carmack* [1989] who, using the same reference salinity (34.8), estimated the average FWC in the deep (interior) Arctic Ocean to be 58,000 km^3. In winter, the FWC in the upper 200 m of the model is higher during the ACCR (43,821 km^3) compared to the CCR (39,929 km^3). Both values are below *Aagaard and Carmack*'s [1989] estimate. On average, the upper 200 m store more fresh water during the ACCR (49,079 km^3) than during the CCR (48,228 km^3). Note that the difference is larger at the end of the regimes.

[33] The Pacific water inflow through the Bering Strait (referred as the Bering Water) affects the upper halocline. One can notice a bulge on the T profiles in Figure 11b caused by relatively warm Bering Water. The temperature maximum is almost absent in the T profile for ACCR April (blue solid line) because the density of the mixed layer is high (Figure 11c) and the Bering Water enters directly into the mixed layer.

3.3.2. Shelf

[34] Shelf water annual salinity increases during the cold anticyclonic regime causing more saline outflow to the Arctic Ocean domain (Figure 12a). Hence, in the ACCR, the shelf contributes more saline water to the interior Arctic Ocean mixed layer. This is another reason, in addition to increased ice production, for higher mixed layer salinity (S_{ml}) in the Arctic Ocean during the ACCR (Figure 10b).

[35] Shelf water outflow is the major source of fresh water to the interior Arctic Ocean mixed layer (Figure 12b). The magnitude of the negative salt flux from the shelf to the mixed layer is greater during the ACCR (up to −5.5 kg m^{-2} yr^{-1} by the end of the ACCR and −4 to −4.2 kg m^{-2} yr^{-1} by the end of the CCR). This stems from higher S_{ml} during the ACCR which amplifies the negative salt flux from the shelf.

3.4. Ice and Ocean Characteristics of the Greenland Sea

[36] The mixed layer in the Greenland Sea model (Figure 13a) is shallower during the cyclonic regime than during the anticyclonic regime. After several years of the CCR forcing the Greenland Sea mixed layer becomes thinner, and at the end of the CCR the maximum convection during the year does not penetrate deeper than 200 m. The mixed layer deepening is determined by the water column stability and buoyancy flux. The stability is characterized by the density jump at the mixed layer lower boundary, i.e., by the mixed layer temperature and salinity (Figure 13b). Interannual variability of the S_{ml} in the Greenland Sea model is controlled by the Polar Water inflow (Q_{PW}) minus the fraction of the outflow from the Arctic Ocean model. It
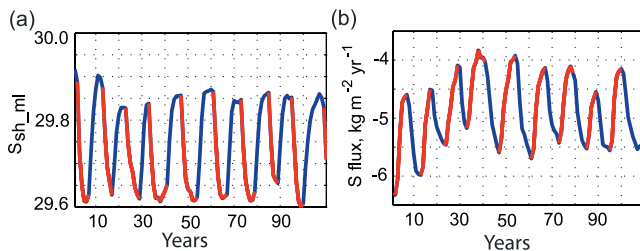

Figure 12. Time series of annual diagnostics from the shelf model. Blue segments denote period of ACCR forcing, red segments CCR forcing. The abscissa is years of integration. (a) Salinity of shelf water outflow to the Arctic Ocean mixed layer. (b) Integrated salt flux to the Arctic Ocean mixed layer.
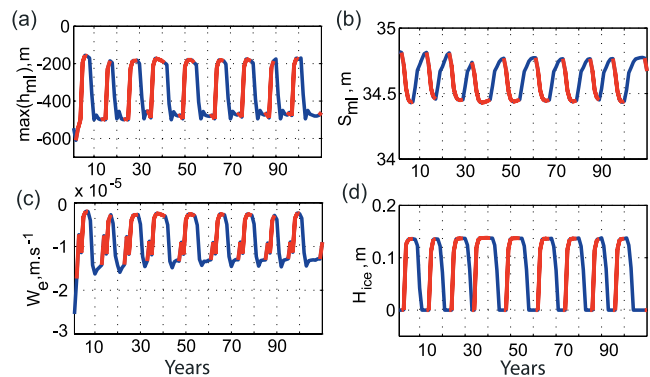

Figure 13. Time series of annual diagnostics from the Greenland Sea model. Blue segments denote period of ACCR forcing, red segments CCR forcing. The abscissa is years of integration. (a) Maximum annual mixed layer depth. (b) Mixed layer salinity. (c) Entrainment velocity. (d) Ice thickness.
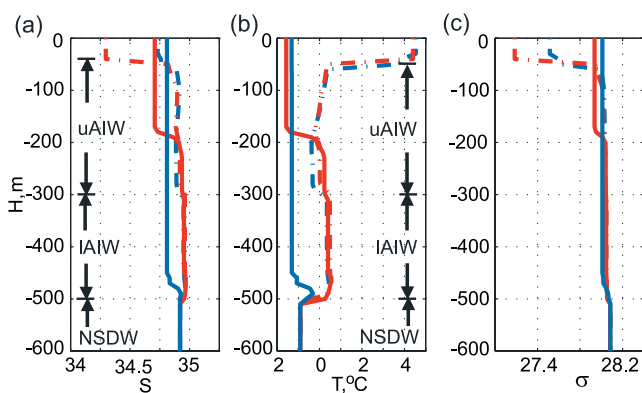
Figure 14. Vertical structure of the upper layer of the simulated Greenland Sea under different regimes. Blue curves correspond to ACCR forcing, red lines to CCR. Solid lines are April profiles, dashed-dotted lines are September profiles. The ordinate is depth. (a) Salinity. (b) Temperature. (c) σ-density. Notations: uAIW – upper Arctic Intermediate Water, lAIW – lower Arctic Intermediate Water, NSDW – Norwegian Sea Deep Water.

has higher values during the CCR causing freshening of the upper layer, damping of deep convection and lower entrainment (Figure 13c).

[37] The entrainment rate largely determines the interannual variability of the mixed layer temperature. During the ACCR, when low water column stability promotes a deeper mixed layer and higher entrainment, the upper Greenland Sea is warmer. During the CCR when the entrainment rate is low, the shallow mixed layer rapidly cools, the mixed layer temperature reaches the freezing point, and ice appears in the Greenland Sea (Figure 13d). Note that the appearance of the ice cover in the Greenland Sea model is related to the intensity of convection, in agreement with other studies [*Pawlowicz*, 1995; *Lenderink and Haarsma*, 1996; *Rudels et al.*, 1999].

[38] Seasonal variability of the Greenland Sea modeled convection is significant (Figure 14). For CCR forcing, the seasonal signal reaches only to 200 m depth (red lines); for the ACCR, it penetrates to 500 m depth (blue lines). Interannual variability in the model is related to this 200 – 500 m convection depth range (blue and red solid lines). Deepening during the ACCR is limited by the depth of the upper boundary of the Norwegian Sea Deep Water (NSDW). It is noteworthy that for the ACCR, the density difference between the mixed layer and underlying water in the April profile is extremely small ($g' = 5.7 \times 10^{-3} \, \text{m}^2 \cdot \text{s}^{-1}$), i.e., the water column is almost neutrally stable and the Greenland Sea is at the pre-convective state. This allows one to assume that under higher values of the surface buoyancy flux which may occur at smaller space scales (for example, intrusion of salt water), chimney convection develops and easily penetrates into the NSDW.

[39] Higher freshwater flux during the CCR decreases density in the upper Greenland Sea while density of the Arctic halocline increases (Figure 11c). During the ACCR, intense deepening of the mixed layer in the Greenland Sea entrains the underlying dense water and increases density in the upper 100 meters. Density of the Arctic halocline decreases at the same time. This causes the growth of the

dynamic height gradient between the two regions during the anticyclonic regime and a decrease during the cyclonic regime (Figure 8a).

4. Discussion

4.1. Interaction Mechanisms in the Modeled System

[40] In this section we discuss how our hypothesis, shown schematically in Figure 3, is realized in the model. Auto-oscillations in the modeled system are achieved through mechanisms (Figure 15) that parallel the hypothesized relations in the Arctic Ocean – GIN Sea climate system (Figure 3). The interaction between the Greenland Sea and the Arctic is realized through the FW flux (described in terms of polar water flow (Q_{PW}) which is a function of the total outflow from the Arctic Ocean model (Q_{g_atl})) and the atmospheric heat advection to the Arctic (F_{adv}). Respectively, these fluxes are controlled by the dynamic height δH and
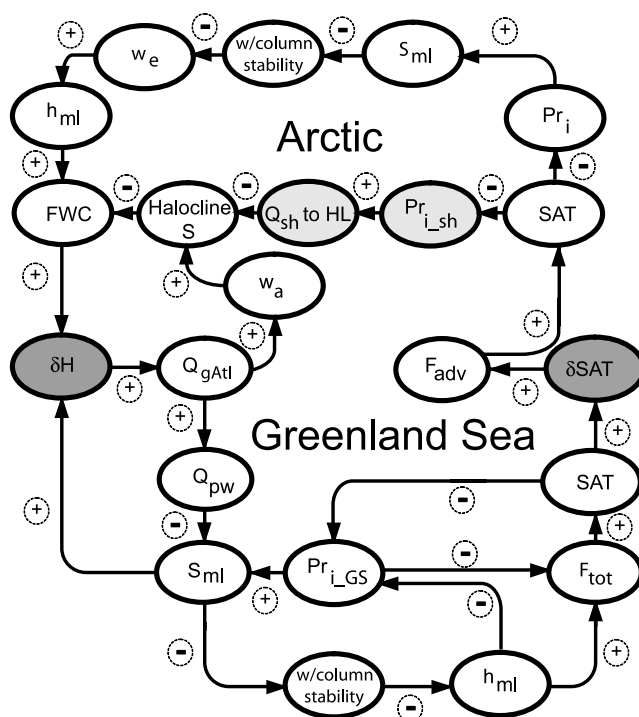

Figure 15. Interaction loop in the simulated climate system. A plus sign denotes mechanisms with positive results; a minus sign denotes mechanisms with negative results. Intensity of atmospheric and oceanic fluxes between the Arctic Ocean and Greenland Sea domains is controlled by dynamic height (δH) and surface air temperature (δSAT) gradients (dark grey cells). Light grey cells mark shelf processes. Other notations: F_{adv} – atmospheric heat flux to the Arctic, SAT – surface air temperature, S_{ml} – mixed layer salinity, w/column stability – stability of water column, w_e – rate of entrainment characterized by entrainment velocity, h_{ml} – mixed layer thickness, FWC – freshwater content, Q_{gAtl} – outflow from the Arctic Ocean, Q_{PW} – polar water inflow to the central Greenland Sea, w_a – vertical velocity, F_{tot} – air-sea surface heat flux, Pr_{i_sh}, Pr_{i_GS} – ice production in the shelf and Greenland Sea sub-models, Q_{sh} to HL – outflow from the shelf domain to the Arctic Ocean halocline.

surface air temperature gradients (δSAT) between the Arctic and GIN Sea modules.

[41] During ACCR, the F_{adv} anomaly is negative, i.e., heat advection to the Arctic is suppressed, which causes negative SAT anomalies to develop in the Arctic (Figure 9b). Negative air temperature anomalies lead to increased ice production (Figure 10d) and increased water salinity (S_{ml}) due to brine rejection (Figure 10b). High S_{ml} reduces water column stability, and the mixed layer thickness (h_{ml}) increases (Figure 10a). Although S_{ml} is higher, the thicker mixed layer and freshening of the halocline (Figure 10a) make FWC of the upper Arctic Ocean higher during the ACCR. Thus, the upper part of the Arctic Ocean becomes less dense and the dynamic height in the Arctic domain grows. In the Greenland Sea model during the ACCR, weak Polar Water outflow causes positive anomalies in the mixed layer salinity (Figure 13b), promoting deeper convection (Figures 14a and 14b) and the dynamic height in the Greenland Sea decreases. As a result, the dynamic height gradient (δH) between the Arctic Ocean and GIN Sea increases (Figure 8a) and forces higher FW outflow to the GIN Sea. The more intense convection initiates stronger heat flux to the winter atmosphere (F_{tot}) which warms the atmosphere (Figures 9a and 9c). Positive SAT anomalies increase the SAT gradient, δSAT (Figure 8b). High δSAT initiates the interaction between the regions (CCR).

[42] During the CCR, strong heat flux to the Arctic increases SAT, intensifies ice melting, freshens the mixed layer, and the mixed layer thickness decreases (due to higher water column stability). A thinner mixed layer and salinification of the halocline decrease FWC in the upper Arctic Ocean and the dynamic height gradient weakens. Anomalously high advection of freshwater to the Greenland Sea during the CCR freshens the upper layer (which further decreases the dynamic height gradient) and increases the water column stability, weakening convection. This leads to negative anomalies in the air-sea fluxes and cooling of the Greenland Sea atmosphere. SAT gradient between the Arctic and Greenland Sea diminishes and interaction fades.

4.2. Decadal Oscillations: Sensitivity to Internal and External Parameters

4.2.1. Period of Oscillations

[43] The period of the oscillations reproduced in the model is determined by the volumes of the Arctic Ocean, shelf, and Greenland Sea regions, vertical temperature and salinity structures in the basins, intensity of FW and heat fluxes in the system, and by the minimum and maximum thresholds of the dynamic height gradient (δH_{min} and δH_{max}). In this study, δH_{min} and δH_{max} were chosen based on two model experiments, run separately under the ACCR and CCR forcing. Shorter or longer time scale oscillations were obtained by reducing or increasing the interval [δH_{min}; δH_{max}]. The oscillatory behavior of the system is clearly sensitive to the values of δH_{min} and δH_{max}. Narrowing this interval, we were able to reproduce oscillations with periods as small as $6-9$ years. A further decrease of the interval led to a non-oscillatory solution (not shown). Similarly, by increasing the interval, longer time scales were obtained ($12-18$ years). However, no oscillations with a period longer than 18 years could be reproduced in this model.

[44] The range of possible periods of the oscillations is wide, from 6 to 18 years, so the results of the model experiment do not prove that the reproduced oscillations have a period of only 10 years. However, this study has shown that the hypothesized oscillations can be generated in the Arctic Ocean – GIN Sea system through the described feedback loop (Figure 3). The necessary conditions that support the auto-oscillations are the delay in the FW and heat fluxes. The system should not respond immediately to a perturbation but has to "accumulate" a disturbance before it transits to the other regime. In the model, this behavior has been introduced by a "switch mechanism" regulating oceanic and atmospheric fluxes depending on the dynamic height gradient between the Arctic Ocean and Greenland Sea modules. The idea of using interbasin dynamic height gradient is supported by the EOF-1 pattern of the dynamic height fields in the Arctic discussed in the Introduction (Figure 4). This mechanism is implemented in the model to parameterize physical processes that cannot be reproduced in our model (e.g., delay in response due to the absence of horizontal dimensions, convergence/divergence of water/ice, etc.).

[45] One problem raised in this paper is whether the hypothesized oscillations are self-sustained (auto-oscillations) or not. Oscillations are considered self-sustained if they are generated inside the system without any periodic forcing from outside; the amplitude and period of the oscillations are determined by system's properties. An auto-oscillating system should possess a source of energy and negative feedback mechanisms that return the system to its initial state. The described Arctic Ocean – GIN Sea climate system does have the energy sources (potential energy accumulated in the Beaufort Gyre and internal energy accumulated in the GIN Sea atmosphere) and negative feedback mechanisms as described earlier. The distribution of energy in the system is controlled by the switch position which, in its turn, depends on the dynamic height gradient between the two modules. Hence, the simulated oscillation is determined by the system and can be viewed as an "auto-oscillation".

[46] The question stays open on how the external forcing can modify, mask or destroy the simulated oscillation. This question touches on the problem of the relation between the AO, NAO, and AOO. The AOO index describes variability only in the Arctic Ocean – GIN Sea region. The NAO describes SLP variability in the North Atlantic. Whether the Arctic can be viewed as a closed system largely depends on the influence of the North Atlantic on this system. If an assumption is made that the coupling between the North Atlantic and the Arctic – GIN Sea system has a long-period (interdecadal or longer) variability, then the following idea can be suggested. When the influence of the North Atlantic on the Arctic is weak, the Arctic Ocean – GIN Sea climate system can be viewed as a closed system and the hypothesized oscillation can exist in its pure form as described above. In this case, the AOO index and the NAO can be weakly correlated and describe the processes in the "isolated" systems. When the influence of the North Atlantic is strong, this system cannot be considered as closed and the hypothesized oscillation would be significantly modified, and the AOO and NAO indices would
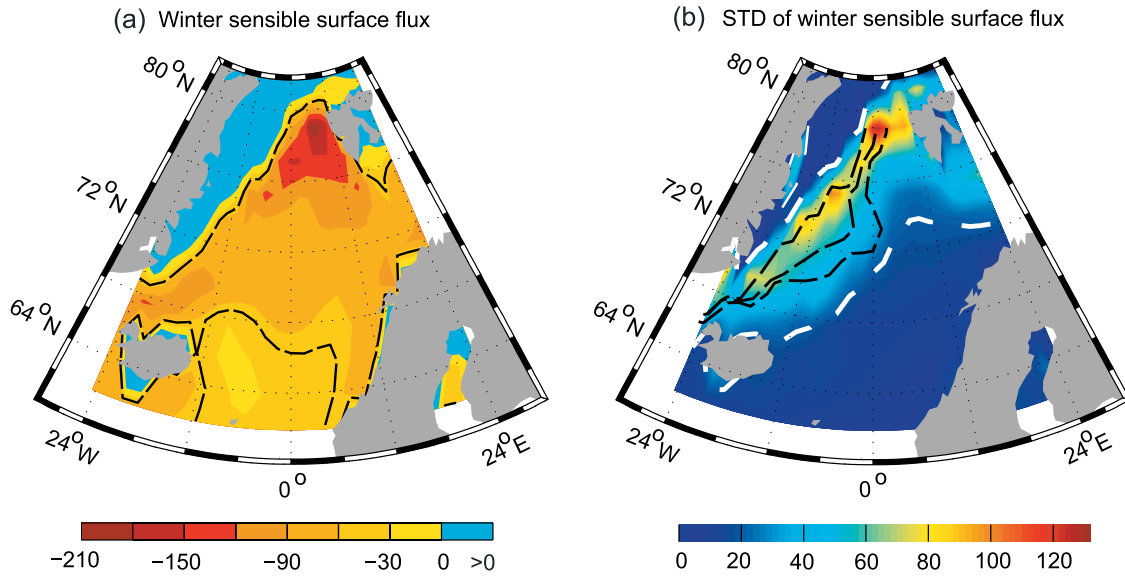
Figure 16. (a) Mean winter (November – March) sensible surface flux in the GIN Sea. The dashed curve marks -50 W·m^{-2}. (b) STD of the mean winter sensible flux in the GIN Sea. (Data are from NCEP Reanalysis fields for 1948–2002, NCAR-CIRES CDC.) The white dashed line is 20 W·m^{-2} isoline. The black dashed curves mark mean winter (November – March) ice edge (ice concentration of 0.2) in the western GIN Sea during years with low (1999) and high (1989) ice concentrations; middle dashed curve is average winter position of the ice edge for years from 1979 to 2003. Monthly ice concentration data are from NCEP/DOF AMIP-II Reanalysis (http://www.cdc.noaa.gov/cdc).

have higher correlation, perhaps similar to what was observed since 1978 (Figure 2).

4.2.2. Role of Heat Fluxes

[47] The Arctic Ocean and shelf models are sensitive to the coefficient of heat advection, χ. For $1.9 \leq \chi \leq 2$ W·m^{-2}·°K^{-1}, the mean Arctic conditions are reproduced in the model. For $\chi > 2$ W·m^{-2}·°K^{-1}, the Arctic and the shelf warm, causing intense ice melting and water freshening. For $\chi < 1.9$ W·m^{-2}·°K^{-1}, the Arctic and shelf box become cold, leading to higher ice production in winter and intense salinification of the upper Arctic Ocean., The simulated annual meridional sensible heat transport to the Arctic, averaged separately over the ACCR and CCR years, was 24.5 W·m^{-2} and 31.7 W·m^{-2}, respectively, resulting in a difference of 7.2 W·m^{-2}. We estimate the area of the Arctic Ocean and the shelf region (excluding the Barents Sea) to be $\sim 0.9 \times 10^{13}$ m^2, which after multiplying by the difference of heat advection, yields a difference in atmospheric meridional heat transport of 65 TW during the ACCR and CCR.

[48] To address whether this difference is real, we first recognize that the GIN Sea basin is a region of extremely strong air-sea heat fluxes [*Häkkinen and Cavalieri*, 1989]. Figure 16a shows the mean winter (November – March) air-sea sensible heat flux (negative to the atmosphere) obtained from NCEP reanalysis data for 1948 – 2002 acquired from NOAA-CIRES CDC (http://www.cdc.noaa.gov). The strongest sensible heat fluxes occur in the central and northern Greenland Sea (-180 to -120 W·m^{-2}). Winter sensible heat flux over the rest of the GIN Sea (excluding the ice covered EGC region) varies from -20 to -120 W·m^{-2}. Variability of the winter sensible heat flux is high over the GIN Sea (Figure 16b) with the values of the

coefficient of variation (standard deviation divided by mean) from -0.6 to -1.2 in the southern GIN Sea to ~ -1.2 to -2.2 in the northern and western GIN Sea (excluding the EGC region). Regions of extremely high variability of heat fluxes coincide with the ice edge position during years of high and low ice concentration in the GIN Sea (black dashed lines on Figure 16b). To compare with our modeled values, we calculated the difference of the winter mean sensible heat flux integrated over the contoured region during years of strong and weak heat fluxes.

[49] We form a random variable X by averaging over the specified region the winter mean sensible heat flux. Noting that X is the spatial average of sample means, from the central limit theorem the distribution of X can be close to the normal distribution:

$$X \sim f(x) = \frac{1}{\hat{\sigma}_X \sqrt{2\pi}} \exp\left[-\frac{(x - \hat{\mu}_X)}{2\hat{\sigma}_X^2}\right] \qquad (3)$$

where $\hat{\mu}_X$ is the ensemble mean sensible flux (estimated from several winters), $\hat{\sigma}_X$ is the estimate of its standard deviation, and x is a particular realization of X (winter heat flux in some year). Assume that we are looking for the minimum difference of the winter mean sensible heat flux during 80% of cold and warm years (ΔX). The difference is found from the following equation:

$$P(x \in \Phi) = 1 - \int_{\hat{\mu}_X - \Delta X/2}^{\hat{\mu}_X + \Delta X/2} f(x)dx = 2 \int_{\hat{\mu}_X + \Delta X/2}^{\infty} f(x)dx = 0.8, \quad (4)$$

where $P(x)$ is the probability that x is from the subspace $\Phi = \{x \leq (\hat{\mu}_X - \frac{\Delta X}{2})\} \cup \{x \geq (\hat{\mu}_X + \frac{\Delta X}{2})\}$ and $f(x)$ is the density

distribution function of X given in equation (3). For the area where winter sensible heat flux is negative and its standard deviation is ≥ 20 W·m^{-2} (white dashed curve on Figure 16b denotes STD = 20), the spatial average flux is -82.8 W·m^{-2} and standard deviation is 49.6 W·m^{-2}. Hence $\hat{\mu}_X = -83$ W·m^{-2} and $\hat{\sigma}_X = 50$ W·m^{-2}, and solving (4) one gets $\Delta X = 25.4$ W·m^{-2}. The area of the specified region in the GIN Sea is 1.2×10^{12} m^2 (total area of the GIN Sea is 2.55×10^{12} m^2 [Aagaard and Carmack, 1989]). This gives a difference between low (below long-term annual mean) and high (above long-term annual mean) fluxes of $\geq 2.97 \times 10^{13}$ W with 0.8 confidence level, almost half the value (6.5×10^{13} W) calculated from the model.

[50] This calculation considers only sensible heat flux which contributes ~30%–40% to the heat loss in the polar regions [Häkkinen and Cavalieri, 1989]. Thus, the total oceanic heat flux in the GIN Sea (inside the dashed curve in Figure 16b) would be at least two to three times higher, well within the amount required for the Arctic Ocean to shift the regime. This shows that the difference in the heat fluxes during years with high and low winter surface fluxes is large and is related to the sea ice concentration in the region (Figure 16b). The difference is sufficient to cause a regime shift in the Arctic Ocean region based on the model estimates.

[51] It should be stressed that the timing in strong and weak heat fluxes to the Arctic domain is essential to generating the oscillation. A simple relation between the heat advection and interbasin temperature gradient (equation (25), part 1) through the coefficient of heat advection (χ) works only when the value of the coefficient is allowed to change for different regimes. Recall that the physical meaning of χ is to regulate the intensity of the meridional heat transport to the Arctic domain mostly via transient eddies (see part 1 for more details). Different values of χ during the ACCR and CCR indicate that the atmosphere over the Arctic undergoes essential changes permitting intense penetration of cyclones into the Arctic during the CCR and reducing their influence on the Polar region during the ACCR.

4.2.3. Role of Freshwater Fluxes

[52] As discussed above, intense heat flux to the Arctic triggers oscillations in the system by inducing anomalies in the Arctic atmosphere-ice-ocean system. The Arctic "responds" with anomalously high freshwater (water and ice) outflow to the Greenland Sea. After the perturbation signal passes through all the components of the interaction loop shown in Figure 3, the system rebuilds the initial state. Thus, the role of freshwater is that it returns the Arctic Ocean – GIN Sea climate system to the state with cold Arctic and warm GIN Sea.

[53] Obviously, different rates of freshwater outflow to the Greenland Sea would result in a different periodicity of oscillations. As mentioned earlier, there are no available observations on the amount of the Polar Water and Atlantic Water (Q_{AtW}) inflowing to the central Greenland Sea. There are speculative, mostly qualitative, estimates showing that the amount of Atlantic Water entering the Greenland Gyre is much higher than the amount of Polar Water [see, e.g., Johannessen, 1986; Swift, 1986; Alekseev et al., 1994]. In this model, the ratio, Q_{PW}/Q_{AtW}, determines the salinity (and consequently, stability) in the upper Greenland Sea. The

results from several model experiments reveal that the annual mean ratio $Q_{PW}/Q_{AtW} \approx 3.7 \times 10^{-2}$ leads to low water column stability in the Greenland Sea model, with highly possible deep convection. For $Q_{PW}/Q_{AtW} \approx 8.0 \times 10^{-2}$, there is strong freshening of the upper Greenland Sea model leading to a shallow mixed layer. A two-fold increase of freshwater flux from the Arctic Ocean to the Greenland Sea simulated in the model provides $Q_{PW}/Q_{AtW} \approx 8.0 \times 10^{-2}$ with intense freshening of the upper Greenland Sea and very shallow mixed layer. It should be mentioned that a change of the ratio Q_{PW}/Q_{AtW} can also be caused by variability in the Atlantic water inflow, which is kept constant in the analyzed model experiment.

[54] Ice volume flux to the Greenland Sea (Q_{mlt_GS}) is another source of fresh water in the domain that has imposed interannual variability. The amount of fresh water gained by the Greenland Sea from this additional flux is very small. For example, during the CCR the average Q_{mlt_GS} is 5046 or 4541 m^3 s^{-1} of liquid fresh water. This is about 0.45% of the polar water inflow to the domain during the CCR. Obviously, this flux is not crucial to support the oscillation; however, it might slightly affect the periodicity.

[55] Freshwater fluxes in the shelf domain determine salinity variations both in the shelf model and in the Arctic Ocean model. River runoff is an important source of freshwater. There is evidence that the Arctic river runoff varies during different regimes [Proshutinsky and Johnson, 1997; Johnson et al., 1999] and might have a noticeable effect on the salinity variations in the upper Arctic Ocean [Johnson and Polyakov, 2001]. In the analyzed model experiment, river runoff has only seasonal variation. Sensitivity analysis of the described model did not reveal any significant changes in the Arctic Ocean salinity simulated with high (for the ACCR) and low (for the CCR) river runoff values suggested in Polyakov et al. [1999]. Salinity variations in the model are mostly controlled by ice freezing/melting variations. The possible explanation could be that variability in the river discharge can cause local salinity variations, which might be significant, depending on where the river plume travels (similar to the case described by Johnson and Polyakov [2001]). Because the oceanic model integrates water characteristics over the whole basin, this model cannot resolve the situation described above.

4.3. Role of Other Factors

[56] Two other factors that participate in generating the oscillation are wind and cloud cover. The wind is necessary in the model to calculate the friction velocity in the mixed layer. During the CCR, when the mixed layer shallows due to stronger stratification, the imposed higher wind speed (Figure 5a) tends to maintain a deep mixed layer. During the ACCR, when the haline convection is strong and the mixed layer becomes thicker, the weaker wind speeds result in weaker wind driven mixing that reduce the mixed layer deepening. In the Greenland Sea domain, the prescribed winds (Figure 5b) support the evolution of deeper and shallower mixed layers as do the other forcing parameters under the ACCR and CCR, respectively. Deepening of the mixed layer is more sensitive to the wind speed in the Greenland Sea model, especially in early spring when the deepening of the mixed layer begins, driven by thermal

convection. The rate of deepening of the mixed layer at this early stage may be crucial for developing the ice cover. The ice appears in the model if the convection cannot overcome the seasonal pycnocline and reach the underlying warm water. Higher wind speeds could provide additional energy sufficient for convection to overcome the density jump. Hence, in this model, interannual variability in the wind forcing mostly affects the period of oscillation, and it has small impact on generating the oscillation itself (see also discussion about wind forcing and wind-related omissions from the model system in section 4.4).

[57] The cloud cover in the Arctic changes for the ACCR and CCR (Figure 6). The presence of an oscillation in the model is not critically dependent on the cloud parameterization; however, it influences the periodicity of the oscillations. Changing cloud cover affects a number of feedback mechanisms in the model system. For example, the higher fraction of cloud cover during the CCR mitigates the effect of increased heat advection from the GIN Sea model by reducing the incoming solar radiation, resulting in slower ice melt. On the other hand, higher cloud cover increases the incoming longwave radiation to the ice promoting ice melt in summer and lower rate of ice freezing in winter.

4.4. Omissions From the Model System

[58] In this study we have not considered some important sources of energy that can contribute to the discussed mechanism of climate variability. The Barents Sea is a significant source of energy in the Arctic with winter monthly turbulent heat fluxes as strong as -400 W·m^{-2} to -600 W·m^{-2} [*Häkkinen and Cavalieri*, 1989]. Variability in the Atlantic water inflow affects the heat budget of the Arctic Ocean [*Zhang et al.*, 1998; *Dickson et al.*, 2000] but it is not clear how much of this heat could escape from the Atlantic layer and reach the sea ice and the atmosphere. Another factor that has not been taken into account in this paper is heat accumulation during summer and heat loss during winter in the Arctic Ocean due to increased amount of open water and thin ice during the CCR [*Aagaard and Carmack*, 1994; *Rigor et al.*, 2002].

[59] Also, the omission of atmosphere, ice and ocean dynamics is a strong simplification of the problem. Atmospheric circulation over the Arctic determines convergence/divergence of the surface water and ice. We speculate that including the dynamics in the system would enhance the simulated oscillation. For example, convergence of the surface water in the central Arctic during the ACCR would significantly increase the dynamic height gradient between the Arctic Ocean and the GIN Sea. All these aspects need further investigation and we plan to study them in the future.

[60] The modeled system has been developed in parallel to the hypothesized Arctic Ocean – GIN Sea climate system which is viewed as a closed system. The model does not consider heat exchange between the Arctic Ocean and the North Pacific and with the continental regions. Though the existence of these fluxes is not argued in this study, they are not considered as crucial for the Arctic Ocean climate as the interaction with the GIN Sea. For example, the major storm track manifested in the SLP distribution over the Arctic Ocean during the cyclonic circulation regimes is the extension of Icelandic Low toward central Arctic. Also in the work of *Dickson et al.* [2000], there is a discussion on the Pacific influences on Arctic climate. The authors argue that the North Pacific index (NP) has a very local influence on the Arctic, mostly, south of the Bering Strait.

5. Conclusions

[61] A simple model of the Arctic Ocean and Greenland Sea coupled to a thermodynamic sea ice model and atmospheric model has been employed to study decadal variability in the ice-ocean-atmosphere climate system. The central hypothesis that motivated the current investigation is based on the theory of the AOO outlined in *Proshutinsky and Johnson* [1997] and *Proshutinsky et al.* [2002]. It states that the behavior of the Arctic Ocean and GIN Sea is auto-oscillatory between two climate states (ACCR and CCR) with quasi-decadal periodicity. The system is characterized by two opposite states: (1) a cold Arctic and warm Greenland Sea region; (2) a warm Arctic and cold Greenland Sea region. When the ACCR dominates the Arctic, the interaction between the two basins is damped, and strong convection in the central Greenland Sea favors intense heat flux to the atmosphere over the Greenland Sea region. These conditions increase the dynamic height gradient between the two regions that ultimately forces them to interact. The CCR is characterized by intense interaction between the basins: the Arctic gains heat advected from the Greenland Sea region and the Greenland Sea receives freshwater released from the Arctic Ocean. This sequence of links and relations between the components of the Arctic Ocean – GIN Sea climate system has been incorporated in the model. From our knowledge of the AOO and analysis of dynamic height gradient fields from the EWG (Figure 4), the interbasin dynamic height gradient is chosen to be an indicator of the simulated regime state. By setting limiting values for the dynamic height gradient, the decadal variability of the observed system can be reproduced by this model. By changing the free parameters, the period of oscillation can be changed within the interval from approximately 6 to 18 years.

[62] The major result of this work is the demonstration of oscillatory behavior of the Arctic Ocean – Greenland Sea climate system. Periodic solutions obtained from simulations with seasonally varying forcing, for scenarios with high and low interaction between the regions, reproduce the major anomalies in the ocean thermohaline structure, sea ice volume, and freshwater fluxes attributed to the ACCR and CCR regimes. The necessary factors to produce the oscillation in the model system are the feedback loop which returns the system to the initial state and a delay mechanism that switches the atmospheric and freshwater fluxes between the basins. The number of necessary limitations and omissions in the model lead us to acknowledge that the simulated oscillation is an idealized case. In particular, the oscillation can exist in the Arctic – GIN Sea system when the system can be viewed as a closed system, i.e., the influence from the North Atlantic is small. Whether the oscillation can be reproduced in the system strongly influenced by the North Atlantic (an open system) has not been investigated in this research.

References

Aagaard, K., and E. C. Carmack (1989), The role of sea ice and other freshwater in the Arctic circulation, *J. Geophys. Res.*, *94*, 14,485–14,498.

Aagaard, K., and E. C. Carmack (1994), The Arctic and climate: A perspective, in *Polar Oceans and Their Role in Shaping the Global Environment*, *Geophys. Monogr. Ser.*, edited by O. M. Johannessen et al., pp. 4–20, AGU, Washington, D. C.

Alekseev, G. V., V. V. Ivanov, and A. A. Korablev (1994), Interannual variability of the thermohaline structure in the convective gyre of the Greenland Sea, in *Polar Oceans and Their Role in Shaping the Global Environment*, *Geophys. Monogr. Ser.*, edited by O. M. Johannessen et al., pp. 485–496, AGU, Washington, D. C.

Ambaum, M. H. P., B. J. Hoskins, and D. B. Stephenson (2001), Arctic Oscillation or North Atlantic Oscillation?, *J. Clim.*, *14*, 3495–3507, doi:10.1175/1520-0442.

Beesley, J. A. (2001), Regional and temporal variations in Arctic cloudiness, in *Proceedings of 6th Conference on Polar Meteorology and Oceanography*, Am. Meteorol. Soc., Boston, Mass.

Beesley, J. A., and R. E. Moritz (1999), Toward an explanation of the annual cycle of cloudiness over the Arctic Ocean, *J. Clim.*, *12*, 395–415.

Belkin, I. M., S. Levitus, J. I. Antonov, and S.-A. Malmberg (1998), Great salinity anomalies in the North Atlantic, *Prog. Oceanogr.*, *41*(1), 1–68.

Björk, G. (1989), A one-dimensional time-dependent model for the vertical stratification of the upper Arctic Ocean, *J. Phys. Oceanogr.*, *19*, 52–67.

Bradley, R. S., and G. H. Miller (1972), Recent climatic change and increased glacierization in the eastern Canadian Arctic, *Nature*, *237*, 385–387.

Budyko, M. I. (1977), *Climate Changes*, 261 pp., Waverly, Baltimore, Md.

Coachman, L. K., and K. Aagaard (1988), Transports through Bering Strait, annual and interannual variability, *J. Geophys. Res.*, *93*, 15,535–15,539.

Deser, C., J. E. Walsh, and M. S. Timlin (2000), Arctic sea ice variability in the context of recent atmospheric circulation trends, *J. Clim.*, *13*, 617–633.

Dickson, R. (1999), All change in the Arctic, *Nature*, *397*, 389–391.

Dickson, R. R., J. Meincke, S.-A. Malmberg, and A. J. Lee (1988), The "Great Salinity Anomaly" in the northern North Atlantic 1968–1982, *Prog. Oceanogr.*, *20*, 103–151.

Dickson, R. R., T. J. Osborn, J. W. Hurrell, J. Meincke, J. Blindheim, B. Adlandsvik, T. Vinje, G. Alekseev, and W. Maslowski (2000), The Arctic Ocean response to the North Atlantic Oscillation, *J. Clim.*, *13*, 2671–2696.

Dukhovskoy, D. S., M. A. Johnson, and A. Proshutinsky (2004), Arctic decadal variability: An auto-oscillatory system of heat and freshwater exchange, *Geophys. Res. Lett.*, *31*, L03302, doi:10.1029/2003GL019023.

Dukhovskoy, D., M. Johnson, and A. Proshutinsky (2006), Arctic decadal variability from an idealized atmosphere-ice-ocean model: 1. Model description, calibration, and validation, *J. Geophys. Res.*, *111*, C06028, doi:10.1029/2004JC002821.

Environmental Working Group (EWG) (1998), *Joint U.S. Russian Atlas of the Arctic Ocean for the Winter/Summer Period* [CD-ROM], Natl. Snow and Ice Data Cent., Boulder, Colo.

Goosse, H., F. M. Selten, R. J. Haarsma, and J. D. Opsteegh (2002), A mechanism of decadal variability of the sea-ice volume in the Northern Hemisphere, *Clim. Dyn.*, *19*, 61–83, doi:10.1007/s00382-001-0209-5.

Gorshkov, S. G. (1980), *Atlas of Oceans: The Arctic Ocean*, Minist. of Def. of the USSR, Moscow.

Häkkinen, S. (1993), Arctic source for Great Salinity Anomaly: A simulation of the Arctic ice ocean system for 1955–1975, *J. Geophys. Res.*, *98*, 16,397–16,410.

Häkkinen, S. (1995), Simulated interannual variability of the Greenland Sea deep water formation and its connection to surface forcing, *J. Geophys. Res.*, *100*, 4761–4770.

Häkkinen, S., and D. J. Cavalieri (1989), A study of oceanic surface heat fluxes in the Greenland, Norwegian, and Barents Seas, *J. Geophys. Res.*, *94*, 6145–6157.

Häkkinen, S., and C. A. Geiger (2000), Simulated low-frequency modes of circulation in the Arctic Ocean, *J. Geophys. Res.*, *105*, 6549–6564.

Häkkinen, S., and A. Proshutinsky (2004), Freshwater content variability in the Arctic Ocean, *J. Geophys. Res.*, *109*, C03051, doi:10.1029/2003JC001940.

Hibler, W. D., III (1979), A dynamic thermodynamic sea ice model, *J. Phys. Oceanogr.*, *9*, 815–846.

Hilmer, M., and T. Jung (2000), Evidence for a recent change in the link between the North Atlantic Oscillation and Arctic sea ice export, *Geophys. Res. Lett.*, *27*(7), 989–992.

Hurrell, J. W., Y. Kushnir, G. Ottersen, and M. Visbeck (Eds.) (2003), *The North Atlantic Oscillation Climatic Significance and Environmental Impact*, 279 pp., AGU, Washington, D. C.

Ikeda, M. (1990), Decadal oscillations of the air-ice-ocean system in the northern hemisphere, *Atmos. Ocean*, *28*, 106–139.

Ikeda, M., J. Wang, and J.-P. Zhao (2001), Hypersensitive decadal oscillations in the Arctic/subarctic climate, *Geophys. Res. Lett.*, *28*, 1275–1278.

Johannessen, O. M. (1986), Brief overview of the physical oceanography, in *The Nordic Seas*, edited by B. G. Hurdle, pp. 103–127, Springer, New York.

Johnson, M. A., and I. V. Polyakov (2001), The Laptev Sea as a source for recent Arctic Ocean salinity changes, *Geophys. Res. Lett.*, *28*, 102,017–102,020.

Johnson, M. A., A. Y. Proshutinsky, and I. V. Polyakov (1999), Atmospheric patterns forcing two regimes of Arctic circulation: A return to anticyclonic conditions?, *Geophys. Res. Lett.*, *26*, 1621–1624.

Jones, P. D., T. M. L. Wigley, and P. B. Wright (1986), Global temperature variations between 1861 and 1984, *Nature*, *322*, 430–434.

Kwok, R., and D. Rothrock (1999), Variability of Fram Strait ice flux and North Atlantic Oscillation, *J. Geophys. Res.*, *104*, 5177–5189.

Lenderink, G., and R. J. Haarsma (1996), Modeling convective transitions in the presence of sea ice, *J. Phys. Oceanogr.*, *26*, 1448–1467.

Lindsay, R. W. (1998), Temporal variability of the energy balance of thick Arctic pack ice, *J. Clim.*, *11*, 313–333.

Makshtas, A. P., E. L. Andreas, P. N. Svyashchennikov, and V. F. Timachev (1999), Accounting for clouds in sea ice models, *Atmos. Res.*, *52*, 77–113.

Marotzke, J., and P. H. Stone (1995), Atmospheric transports, the thermohaline circulation, and flux adjustments in a simple coupled model, *J. Phys. Oceanogr.*, *25*, 1350–1364.

Maslanik, J., M. C. Serreze, and R. G. Barry (1996), Recent decrease in Arctic summer ice cover and linkages to atmospheric anomalies, *Geophys. Res. Lett.*, *23*, 1677–1680.

Moon, S., and M. Johnson (2005), The relationship between the 0C isotherm and atmospheric forcing in the Arctic Ocean, *Geophys. Res. Lett.*, *32*, L20608, doi:10.1029/2005GL023213.

Mysak, L. A., and S. B. Power (1992), Sea-ice anomalies in the western Arctic and Greenland-Icelandic Sea and their relation to an interdecadal climate cycle, *Clim. Bull.*, *26*, 147–176.

Mysak, L. A., and S. A. Venegas (1998), Decadal climate oscillations in the Arctic: A new feedback loop for atmospheric-ice-ocean interactions, *Geophys. Res. Lett.*, *25*(19), 3607–3610.

Pawlowicz, A. (1995), A note on seasonal cycles of temperature and salinity in the upper waters of the Greenland Sea Gyre from historical data, *J. Geophys. Res.*, *100*, 4715–4726.

Polyakov, I. V., and M. A. Johnson (2000), Arctic decadal and interdecadal variability, *Geophys. Res. Lett.*, *27*, 4097–4100.

Polyakov, I. V., A. Y. Proshutinsky, and M. A. Johnson (1999), Seasonal cycles in two regimes of Arctic climate, *J. Geophys. Res.*, *104*, 25,761–25,788.

Proshutinsky, A. Y., and M. A. Johnson (1997), Two circulation regimes of the wind-driven Arctic Ocean, *J. Geophys. Res.*, *102*, 12,493–12,514.

Proshutinsky, A. Y., I. V. Polyakov, and M. A. Johnson (1999), Climate states and variability of Arctic ice and water dynamics during 1946–1997, *Polar Res.*, *18*, 135–142.

Proshutinsky, A. Y., et al. (2001), Multinational effort studies differences among Arctic Ocean models, *Eos Trans. AGU*, *82*(51), 637, 643–644.

Proshutinsky, A. Y., R. H. Bourke, and F. A. McLaughlin (2002), The role of the Beaufort Gyre in Arctic climate variability: Seasonal to decadal climate scales, *Geophys. Res. Lett.*, *29*(23), 2100, doi:10.1029/2002GL015847.

Proshutinsky, A. Y. (2005), Arctic Ocean Study: Synthesis of model results and observations, *Eos Trans. AGU*, *86*(40), 368, doi:10.1029/2005EO400003.

Rigor, I. G., R. Colony, and S. Martin (2000), Variations in surface air temperature observations in the Arctic, 1979–97, *J. Clim.*, *13*, 896–914.

Rigor, I. G., J. M. Wallace, and R. Colony (2002), Response of sea ice to the Arctic Oscillation, *J. Clim.*, *15*, 2648–2663.

Rogers, J. C. (1997), North Atlantic storm track variability and its association to the North Atlantic oscillation and climate variability of northern Europe, *J. Clim.*, 10, 1635–1647.

Rudels, B., H. J. Friedrich, D. Hainbucher, and G. Lohman (1999), On the parameterization of oceanic sensible heat loss to the atmosphere and to ice in an ice-covered mixed layer in winter, *Deep Sea Res., Part II*, 46, 1385–1425.

Serreze, M. C., F. Carse, and R. G. Barry (1997), Icelandic Low cyclone activity: Climatological features, linkages with the NAO, and relationships with recent changes in the Northern Hemisphere circulation, *J. Clim.*, 10, 453–464.

Steele, M., W. Ermold, S. Hakkinen, D. Holland, F. K. M. Karcher, W. Maslowski, N. Steiner, and J. Zhang (2001), Adrift in the Beaufort Gyre: A model intercomparison, *Geophys. Res. Lett.*, 28, 2935–2938.

Suarez, M. J., and P. S. Schopf (1988), A delayed action oscillator for ENSO, *J. Atmos. Sci.*, 45, 3283–3287.

Swift, J. H. (1986), The Arctic waters, in *The Nordic Seas*, edited by B. G. Hurdle, pp. 129–153, Springer, New York.

Thomas, D., S. Martin, D. Rothrock, and M. Steele (1996), Assimilating satellite concentration data into an Arctic sea ice mass balance model, 1979–1985, *J. Geophys. Res.*, 101, 20,849–20,868.

Thompson, D. W. J., and J. M. Wallace (1998), The Arctic Oscillation signature in the wintertime geopotential height and temperature fields, *Geophys. Res. Lett.*, 25, 1297–1300.

van Loon, H., and J. C. Rogers (1978), The seesaw in winter temperatures between Greenland and Northern Europe. Part I: General description, *Mon. Weather Rev.*, 106, 296–310.

Venegas, S. A., and L. A. Mysak (2000), Is there a dominant timescale of natural climate variability in the Arctic?, *J. Clim.*, 13, 3412–3434.

Vinje, T., and O. Finnekasa (1986), The ice transport through the Fram Strait, *Skrift. Norg. Polarinst.*, 186, 1–39.

Vinje, T., T. B. Loyning, and I. Polyakov (2002), Effects of melting and freezing in the Greenland Sea, *Geophys. Res. Lett.*, 29(23), 2129, doi:10.1029/2002GL015326.

Vinnikov, K. Y., A. Robock, R. J. Stouffer, J. E. Walsh, C. L. Parkinson, D. J. Cavalieri, J. F. B. Mitchell, D. Garrett, and V. F. Zakharov (1999), Global warming and Northern Hemisphere sea ice extent, *J. Clim.*, 286, 1934–1937.

Wadhams, P. (1994), Sea ice thickness changes and their relation to climate, in *Polar Oceans and Their Role in Shaping the Global Environment*, *Geophys. Monogr. Ser.*, edited by O. M. Johannessen et al., pp. 337–361, AGU, Washington, D. C.

Walker, G. T. (1924), Correlation in seasonal variation of weather, *IX Mem. Ind. Met. Dept.*, 25, 275–332.

Zhang, J., D. A. Rothrock, and M. Steele (1998), Warming of the Arctic Ocean by a strengthened Atlantic inflow: Model results, *Geophys. Res. Lett.*, 25, 1745–1748.

————————————

D. Dukhovskoy, Center for Ocean-Atmospheric Prediction Studies, Florida State University, Tallahassee, FL 32306, USA. (ddmitry@coaps.fsu.edu)

M. Johnson, Institute of Marine Science, University of Alaska Fairbanks, Fairbanks, AK 99775, USA.

A. Proshutinsky, Physical Oceanography Department, Woods Hole Oceanographic Institution, Woods Hole, MA 02543, USA.